ACADÉMIE
DES SCIENCES
INSTITUT DE FRANCE

Comptes Rendus
Mécanique

Duc Nguyen Minh, Thom Do Van and Minh Phung Van

An analytical method for nonlinear thermo-mechanical buckling evaluation of functionally graded circular microplates

Volume 354 (2026), p. 293-312

Online since: 15 April 2026

https://doi.org/10.5802/crmeca.353

The Comptes Rendus. Mécanique *are a member of the Mersenne Center for open scientific publishing*
www.centre-mersenne.org — e-ISSN : 1873-7234

ACADÉMIE DES SCIENCES
INSTITUT DE FRANCE

Comptes Rendus. Mécanique
2026, Vol. 354, p. 293-312
https://doi.org/10.5802/crmeca.353

Research article

An analytical method for nonlinear thermo-mechanical buckling evaluation of functionally graded circular microplates

Duc Nguyen Minh [a], **Thom Do Van** [a] **and Minh Phung Van** [*, a]

[a] Department of Solid Mechanics, Faculty of Mechanical Engineering, Le Quy Don Technical University, 236 Hoang Quoc Viet Street, Nghia Do Ward, Hanoi, 100000, Vietnam

E-mails: minhpv@lqdtu.edu.vn, minhpv.mta@gmail.com (M. Phung Van)

Abstract. This paper analytically investigates the nonlinear static buckling behavior of functionally graded (FG) circular microplates by integrating Kirchhoff plate theory, von Kármán geometric nonlinearity, and the modified couple stress theory to account for size-dependent effects. The microplate is concurrently exposed to a uniform pressure and a uniformly increasing through-thickness thermal load. A method based on displacement is used, where the expected movement and bending of the plate are described using polynomial functions that fit the fixed edges of the plate. This choice reduces computational cost while maintaining sufficient accuracy in predicting the nonlinear structural response. By using the Ritz energy method, we can derive straightforward formulas for the critical thermal buckling load and how the load relates to deflection after buckling for the FG circular microplate. The numerical results show that changes in the volume fraction index, material length-scale parameter, and shape features are very important in determining how strong the FGM structure is against buckling and how it behaves after buckling. The results give important insights and serve as a helpful guide for designing microscale functionally graded structures that experience both heat and mechanical stress.

Keywords. FGM circular microplate, Nonlinear thermal buckling, Von Kármán nonlinearity, Modified couple stress theory, Size-dependent effect, Post-buckling behavior.

Funding. Le Quy Don Technical University Research Fund under code 25.01.14.

Manuscript received 13 January 2026, revised and accepted 26 February 2026, online since 15 April 2026.

1. Introduction

In recent years, functionally graded materials (FGMs) have received considerable attention because they enable smooth variations in material properties, leading to improved thermo-mechanical performance compared with conventional laminated composites. FGMs can effectively alleviate problems like stress concentration, delamination, and thermal mismatch by customizing the spatial distribution of constituent phases, usually ceramic and metal, rendering them especially appropriate for advanced engineering applications in aerospace, microelectronics, energy systems, and high-temperature settings [1]. As structural components diminish to the micro-scale, the integration of material length-scale effects is crucial for precise predictions of

* Corresponding author

mechanical reactions. The modified couple stress theory (MCST) introduces a single intrinsic length-scale parameter and has been widely employed to describe size-dependent behavior in micro- and nano-scale structures with reasonable mathematical simplicity [2].

Circular plates are a key category of structural elements extensively used in the design of micro-devices, sensors, actuators, and thermal protection components. The stability characteristics of plates made from functionally graded materials (FGMs) may exhibit significant nonlinearity when operating in situations with concurrent mechanical and thermal loads, particularly under considerable deflections. Traditional plate theories, while sufficient for macro-scale assessments, often neglect the synergistic effects of geometric nonlinearity, material gradation, and size dependency that govern the behavior of micro-scale structures. Therefore, a comprehensive theoretical framework that incorporates von Kármán geometric nonlinearity, through-thickness material gradation, and microscale effects is required to accurately capture buckling and post-buckling responses. Using the Moore–Gibson–Thompson thermal conduction model, Tiwari et al. [3] analyzed the visco-thermoelastic vibration behavior of circular microplate resonators and showed that accounting for finite thermal wave speeds and relaxation effects leads to vibration and damping characteristics that differ markedly from those predicted by classical Fourier-based models. Lin et al. [4] investigated vibration-based energy harvesting in functionally graded circular microplates reinforced with carbon nanotubes and integrated piezoelectric layers, and demonstrated that both material gradation and nanotube reinforcement markedly enhance electromechanical conversion efficiency, which is critical for advanced energy harvesting applications. Thermo-viscoelastic phenomena in microplates have been thoroughly investigated. Abouelregal and colleagues [5] examined the thermoviscoelastic responses of Kirchhoff circular microplates using the MGT model enhanced by modified couple stress theory, demonstrating that size effects and hyperbolic heat conduction substantially affect transient thermal stresses. Do, Ong, and Lee [6] analyzed the nonlinear thermal buckling behavior of porous microplates reinforced with graphene platelets and showed that both graphene content and porosity distribution play a significant role in governing post-buckling stability, especially under high-temperature conditions. Flexoelectric and spinning microplate devices have garnered renewed interest. Hosseini et al. [7] performed a vibration study of rotating annular flexoelectric microplates, demonstrating that rotation and flexoelectric coupling together result in significant stiffening and frequency alterations. Li and Qing [8] investigated the size-dependent axisymmetric buckling and free vibration behavior of functionally graded piezomagnetic microplates based on a nonlocal integral polar model, and demonstrated that the integral formulation yields more physically consistent predictions than corresponding differential models. Recent developments in constitutive modeling have contributed significantly to the improvement of microplate theories. In this context, Ahmadi, Fathalilou, and Rezazadeh [9] employed a Neo-Hookean hyperelastic formulation to analyze the coupled nonlinear response of circular microplates supported by micro-pillars, thereby offering deeper physical insight into pronounced geometric and material nonlinearities. In addition to mechanics, Yuan and colleagues [10] investigated asymmetric optical waveguides using organic microplates, underscoring their significance in micro-optical and photonic device engineering. Advanced computational methods and high-order theories have likewise enhanced the comprehension of microplate dynamics. Hung et al. [11] used a modified strain gradient theory with isogeometric analysis to investigate FG triply periodic minimum surface (TPMS) microplates, demonstrating that microstructural periodicity and strain gradient effects considerably influence frequency spectra. Harazono and colleagues [12] assessed the accuracy of microplate handling in robotic laboratory automation systems, providing practical insights into microplate dynamics in actual operating situations. Thermoelastic damping, an essential element for micro- and nano-resonators, has been thoroughly examined in recent scholarly works. Xiao et al. [13] proposed a generalized thermoelasticity formulation to analyze

thermoelastic damping in circular nanoplates and showed that the damping behavior is highly sensitive to relaxation times and nonlocal heat conduction effects. Peng and colleagues [14] examined the memory-dependent and small-scale influences on the thermoelastic damping of composite microplates enhanced with graphene nanoplatelets, establishing that visco-thermal memory and nano-reinforcement enhance damping properties at operating frequencies. Peng et al. [15] analyzed size-dependent thermoelastic damping in functionally graded graphene-reinforced microplates based on the Moore–Gibson–Thompson model and demonstrated that material gradation and higher-order heat transport mechanisms have a pronounced influence on resonant quality factors. Liu and colleagues [16] investigated the symmetric and asymmetric vibrational properties of bi-directionally graded annular microplates, revealing that directional gradation significantly influences modal interaction and frequency separation, crucial aspects in micro-resonator design. Ansari and colleagues [17] developed an analytical solution for the nonlinear buckling and postbuckling behavior of cylindrical nanoshells using surface elasticity theory, demonstrating that surface energy effects significantly modify the critical load and post-buckling trajectory at the nanoscale. Ansari and colleagues [18] expanded size-dependent modeling to microplates, examining the thermal buckling of Mindlin rectangular FGM microplates through the lens of strain gradient theory and demonstrating the significant impact of material gradation and intrinsic length scale parameters on thermal stability. Gholami and colleagues [19] studied how the size affects the free vibration and buckling of magneto-electro-thermo-elastic nanoplates using a special plate model, showing how both nonlocal effects and field interactions together impact the structure's behavior.

Although numerous studies have examined the mechanical and thermal buckling behavior of functionally graded plates at the macroscale, relatively few investigations have focused on circular microplates that explicitly incorporate size-dependent effects. Current literature often depends on higher-order shear deformation theories, numerical discretization methods, or simple linearized models, which might be computationally intensive or inadequate for accurately representing nonlinear behavior in the post-buckling phase. In addition, the availability of analytical solutions for functionally graded circular microplates under combined thermo-mechanical loading remains scarce because of the highly nonlinear nature of the governing equations. Jain et al. [20] developed a meshfree formulation for analyzing size-dependent thermal buckling and post-buckling behavior of porous microplates resting on elastic foundations, and demonstrated that strong coupling exists among porosity, temperature gradients, and foundation stiffness under localized heating. Likewise, Chen and his study team [21] examined the thermal buckling of graphene platelet-reinforced composite micro smart plates on elastic foundations, demonstrating that GPL reinforcement and thermal loading substantially affect critical buckling temperatures. Tran et al. [22] proposed an advanced iBCMO-DNN algorithm for the stochastic thermal buckling analysis of functionally graded porous microplates based on modified strain gradient theory, and showed that the approach achieves high accuracy in capturing variability in material properties, geometric parameters, and temperature fields. Advanced modeling of thermoelastic and thermo-viscoelastic behavior continues to enhance the understanding of microplate systems. Liu and other researchers [23] used artificial neural networks to study the heat buckling of microplates with graphene platelets and integrated piezoelectric layers. This gave them accurate and computationally efficient predictions. Zhang et al. [24] analyzed the thermal buckling, free vibration, and transient behavior of rotating porous microbeams reinforced with graphene nanoplatelets and showed that temperature effects, porosity, and rotational motion interact strongly to influence the structural response. Joueid et al. [25] further investigated on thermoelastic buckling in plates and shells made of functionally graded materials that rely on temperature and porosity. They found that critical buckling conditions are very sensitive to changes in temperature and porosity. Recent research also examines smart sandwich architectures and microplates

including sophisticated multiphysics couplings. Qin et al. [26] conducted numerical analyses to evaluate the critical buckling temperatures of sandwich microplates with cellular cores and CNT-reinforced piezoelectric patches, and showed that core topology, electromechanical reinforcement, and length-scale parameters significantly affect buckling behavior based on modified strain gradient theory. Tang et al. [27] investigated the size-dependent vibration and buckling behavior of porous functionally graded microplates in thermal environments based on modified couple stress theory. The dual power-law distribution of scale parameters helped them understand how microstructural and thermal effects interact. Salari and Vanini [28] analyzed the nonlocal nonlinear static and dynamic snap-through buckling behavior of thermally post-buckled imperfect functionally graded circular nanoplates and demonstrated that temperature effects, initial imperfections, and nonlocal elasticity strongly govern the nonlinear response. Several recent studies have looked at how stress, displacement, and instability patterns change with size in different microplate layouts. Liu and colleagues [29] evaluated the impact of thermal loads and micro-scale factors on stress/strain/displacement distributions, validating notable discrepancies in microscale responses relative to conventional expectations. Wen and other researchers [30] created models of double-layered microplate systems that took into account couple stress effects and interlayer interactions. These models showed the circumstances under which buckling mode changes happen. Tran et al. [31] proposed advanced computational methods for the analysis of vibration, buckling, and transient responses of porous metal-foam microplates. They showed that porosity and heat fields work together to control dynamic properties. Additional understanding of thermal buckling in multi-directional and curved microscale shells has been attained. Daikh and colleagues [32] examined porous functionally graded material (FGM) configurations in sandwich nanoplates subjected to heat conduction through nonlocal strain gradient theory, revealing that porosity distribution and small-scale factors significantly affect thermal buckling resistance. Farajpour and colleagues [33] introduced a higher-order plate model that incorporates nonlocal effects and strain gradients for orthotropic nanoplates exposed to thermal conditions, highlighting the interplay between nonlocal softening and strain gradient stiffening mechanisms in influencing the critical buckling load. Bouazza [34] created a detailed model to study how functionally graded rectangular plates bend under heat at a larger scale, using a method that improves accuracy in showing how shear forces work without needing extra correction factors. Khuat Duc et al. [35] developed an isogeometric modeling framework with variable length-scale parameters to analyze the dynamic buckling behavior of thermally loaded doubly curved, bidirectional functionally graded porous shallow microshells, and showed that curvature, material gradation, and porosity strongly influence the buckling response. Li et al. [36] investigated the vibro-acoustic response of functionally graded sandwich microplates under coupled thermal-electric loading and demonstrated that strong interactions exist between vibro-acoustic behavior, material gradation, and thermo-electrical fields. Marin et al. [37] investigated the impact of internal rotations and alterations in material structure on the initial boundary value issue of thermoelastic bodies, demonstrating that the incorporation of microstructural elements significantly modifies the propagation and behavior of thermoelastic fields. Their research has shown that employing sophisticated continuum theories is essential for precisely modeling materials when conventional thermoelastic concepts are insufficient. From a computational mechanics perspective, Vlase, Negrean, and their colleagues [38] proposed an energy-based method that employs the concept of acceleration energy to formulate motion equations within a three-dimensional finite element framework. This approach established a robust energy foundation for formulating dynamic equations and enhanced the stability and reliability of finite element modeling. Recently, Abouelregal et al. [39] examined the impact of a specialized heat transfer model, which accounts for historical influences, on thermoelastic materials, demonstrating that these factors substantially alter the behavior of heat waves and stress.

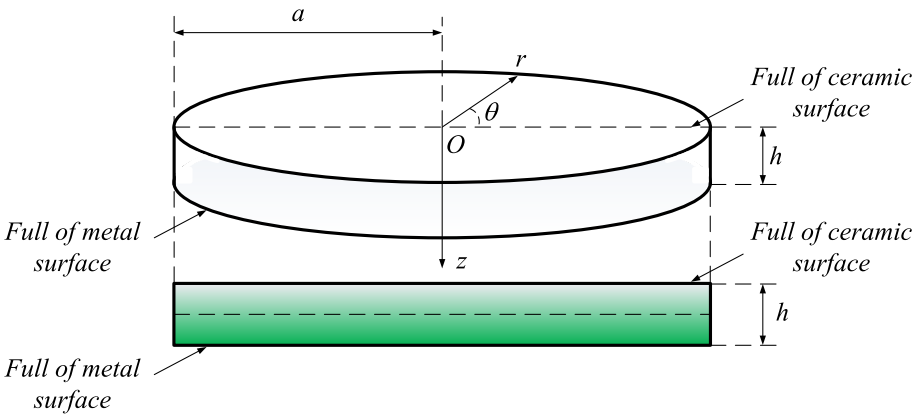

Figure 1. Structural model of the FGM circular microplate.

In this study, the governing equations of a functionally graded circular microplate are formulated based on Kirchhoff plate theory combined with modified couple stress theory and von Kármán-type nonlinear strain–displacement relations. A displacement-based methodology using polynomial shape functions that adhere to clamped boundary constraints is used to guarantee analytical tractability and enhanced precision. By applying the Ritz energy method, accurate expressions for the critical thermal buckling load and the nonlinear post-buckling load–deflection relationships are derived. A parametric study is performed to investigate how the FGM volume fraction index, intrinsic length-scale parameter, plate geometry, and thermal loading influence the stability behavior of the microplate. The findings provide enhanced insight into the nonlinear thermo-mechanical behavior of functionally graded material microplates and present practical recommendations for the optimum design of micro-scale structural components subjected to coupled loading conditions.

The remainder of this paper is organized as follows. Section 2 presents the governing equations of the functionally graded circular microplate, in which the MCST, the formulation of the FGM circular microplate, and the corresponding mechanical relations are described in detail. Section 3 provides a comparative study to validate the proposed model. Section 4 presents numerical investigations along with detailed discussions of the results. Section 5 summarizes the main conclusions and significant findings of this study.

2. Governing equations of a functionally graded circular microplate

The functionally graded circular microplate considered in this study is treated as a thin elastic structure with deformable behavior, as illustrated in Figure 1. The plate is characterized by a radius a and a uniform thickness h. A cylindrical coordinate system (r,θ,z) is employed, with the origin located at the center of the mid-surface and lying on the $r\theta$-plane. The microplate is subjected to a uniformly distributed transverse load $q(r)$. Its kinematic behavior is governed by the von Kármán nonlinear plate theory, whereas size-dependent material behavior is captured using the modified couple stress theory.

In this work, the earlier-mentioned assumptions are used throughout the model development, including the derivation of the strain–displacement relations, the MCST constitutive equations, the energy functional, and the application of the Ritz method. The model's applicability is restricted to small strains, moderate rotations, and linear elastic material behavior to ensure mechanical consistency.

2.1. *Modified couple stress theory*

According to the modified couple stress theory [40], the strain energy U_{int} of a linear elastic isotropic material occupying the domain V is expressed as follows:

$$U_{\text{int}} = \frac{1}{2}\int_V \left(\sigma : \varepsilon + m : \chi\right) \mathrm{d}V, \tag{1}$$

Here, ε, χ, m (conjugate to χ) represent the strain tensor, symmetric curvature tensor, and the deviatoric component of the couple-stress tensor, respectively, which are defined by the following relations [40]:

$$\varepsilon = \tfrac{1}{2}\left[\nabla u + (\nabla u)^T\right], \tag{2}$$

$$\chi = \tfrac{1}{2}\left[\nabla \theta + (\nabla \theta)^T\right], \tag{3}$$

$$\sigma = \lambda \operatorname{tr}(\varepsilon) I + 2\mu\varepsilon, \tag{4}$$

$$m = 2l^2\mu\chi. \tag{5}$$

Here, λ and μ denote the Lamé constants, while l represents the intrinsic material length-scale parameter. This parameter is mathematically defined as the square root of the ratio between the curvature modulus and the shear modulus and characterizes the magnitude of couple-stress effects [41]. The symbol I denotes the identity tensor. The displacement vector u is related to the rotation vector θ by:

$$\theta = \tfrac{1}{2}\operatorname{curl} u. \tag{6}$$

Compared with the classical theory, the modified couple stress theory is distinguished by the use of a symmetric couple-stress tensor and the introduction of only one intrinsic material length-scale parameter together with the conventional Lamé constants [40,41].

The stress tensor in Equation (4) and the couple-stress tensor in Equation (5) are formulated under the plane-stress assumption. By expressing the Lamé constants in terms of the Young's modulus $E(z)$ and Poisson's ratio υ, the constitutive relations can be rewritten as follows [42]:

$$\sigma_{\alpha\beta} = \frac{E(z)}{1-\upsilon^2}\left[\upsilon\varepsilon_{kk}\delta_{\alpha\beta} + (1-\upsilon)\varepsilon_{\alpha\beta}\right], \quad m_{\alpha\beta} = 2Gl^2\chi_{\alpha\beta} \tag{7}$$

where the Lamé constants λ and μ are replaced by the elastic modulus $E(z)$ and Poisson's ratio υ. The equations $\lambda = E(z)\cdot\nu/[(1+\nu)(1-2\nu)]$ and $\mu = G = E(z)/[2(1+\nu)]$ show how they are related. The letter G stands for the shear modulus, while the letter δ_{ij} signifies the Kronecker delta.

The MCST is an improved model of classical elasticity that adds an extra part to the strain energy based on curvature and a specific material length-scale parameter. This analysis assumes the material behaves in a straightforward elastic way, with any nonlinearity coming only from how strain relates to displacement based on the von Kármán formulation. Since the strains are small and the stress–strain relationships in MCST stay linear, the idea of total potential energy still holds true. As a result, combining MCST with geometric nonlinearity makes sense for studying buckling and what happens after buckling.

2.2. *FGM circular microplate*

Functionally graded materials are commonly fabricated by combining ceramic and metallic constituents or by integrating multiple metallic phases. The ceramic phase typically exhibits low thermal conductivity and high temperature resistance. The ductile metallic phase, on the other hand, helps prevent brittle fracture under steep temperature gradients [1].

A power-law function is adopted to describe the through-thickness variation of the metal and ceramic volume fractions, denoted by V_{m} and V_{c}, respectively [43]:

$$V_{\text{c}} = \left(\frac{2z+h}{2h}\right)^k, \quad V_{\text{m}} = 1 - V_{\text{c}}, \quad k \geq 0, \quad k = \text{infinity}. \tag{8}$$

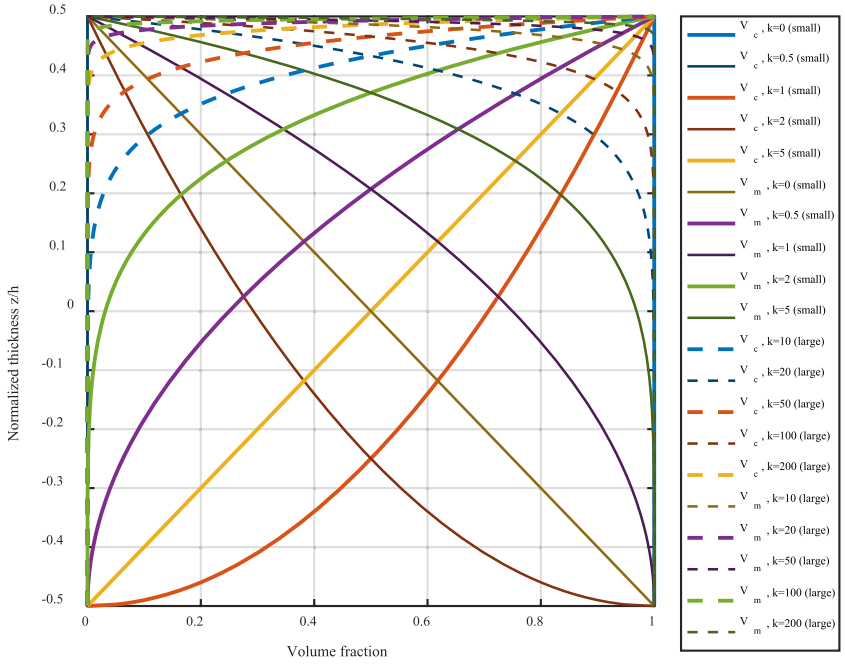

Figure 2. Power-law distribution of V_c and V_m through microplate thickness.

In this formulation, z denotes the thickness coordinate within the range $-h/2 \le z \le h/2$, h represents the plate thickness, and k is the volume fraction exponent with non-negative values. A linear variation of ceramic and metal constituents through the thickness is obtained when $k = 1$, whereas the plate becomes fully ceramic for $k = 0$. The corresponding thickness-wise distributions of V_c and V_m governed by the power-law function are illustrated in Figure 2.

The behavior of functionally graded materials is strongly influenced by the volume fraction distribution of their constituents. In this study, the elastic modulus $E(z)$ and thermal expansion coefficient α are modeled as thickness-dependent properties governed by the Voigt mixture rule [44], while Poisson's ratio ν is assumed to remain unchanged through the thickness [45], as presented below:

$$E(z) = E_c V_c(z) + E_m V_m(z), \tag{9}$$

$$\alpha(z) = \frac{\alpha_c E_c V_c(z) + \alpha_m E_m V_m(z)}{E(z)}. \tag{10}$$

In many FGM plate models, Poisson's ratio ν is treated as thickness-independent. This simplification is motivated by the relatively minor variation of ν compared to the elastic modulus and thermal expansion coefficient, as well as its limited influence on the overall bending stiffness and buckling response. Such an assumption is consistent with earlier investigations on FGM structures [45].

The thickness-dependent profiles of the elastic modulus and thermal expansion coefficient are depicted in Figure 3.

2.3. *Strain–displacement relationship*

In the axisymmetric analysis of the functionally graded circular microplate, the Kirchhoff plate theory is employed to express the displacement components (u_r, u_θ, u_z) in terms of the

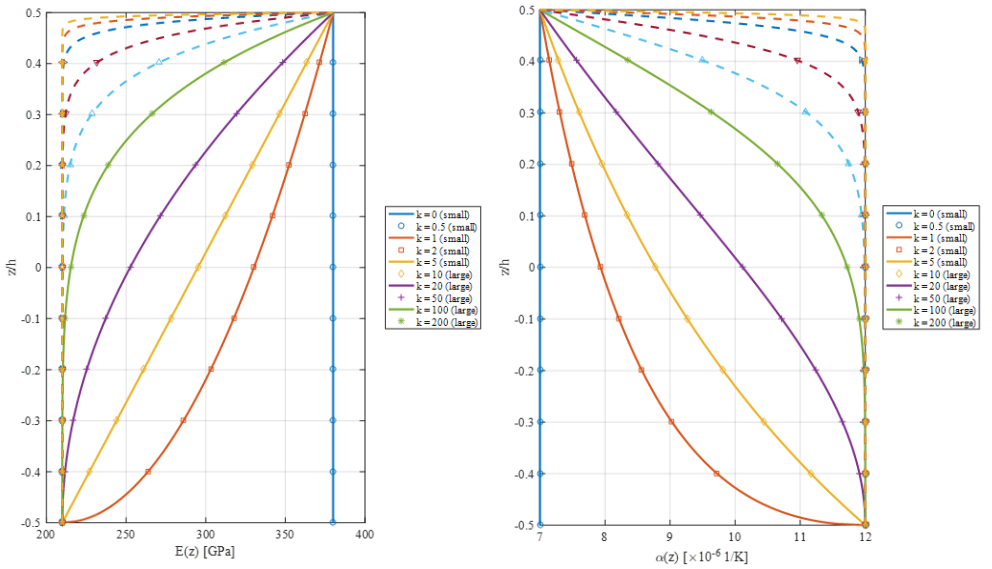

a) $E(z)$ b) $\alpha(z)$

Figure 3. Elastic modulus and thermal expansion coefficient distributions.

displacements of a point on the plate's neutral surface [46]:

$$u_r(r,z) = u(r) - z w_{,r}(r), \quad u_\theta(r,z) = 0, \quad u_z(r,z) = w(r). \tag{11}$$

here, $u(r)$ and $w(r)$ represent the radial and transverse displacements of a point located on the neutral surface of the plate, respectively, where the radial coordinate r varies from 0 to a. Partial derivatives with respect to r are indicated by a comma followed by the corresponding subscript.

When a circular plate undergoes large axisymmetric deformation, the nonlinear strain components that are nonzero according to the von Kármán equation are written as [47]:

$$\varepsilon_{rr}(r,z) = u_{,r} + \frac{1}{2} {w_{,r}}^2 - z w_{,rr}, \quad \varepsilon_{\theta\theta}(r,z) = \frac{u}{r} - z\frac{1}{r} w_{,r}. \tag{12}$$

Based on the displacement field defined in Equation (11), the only non-vanishing component of the rotation vector and the corresponding symmetric curvature tensor are obtained from Equations (3) and (6) and can be written in polar coordinates as:

$$\theta_\theta = -w_{,r}, \quad \chi_{r\theta} = \frac{1}{2}\left(\frac{1}{r} w_{,r} - w_{,rr}\right). \tag{13}$$

2.4. *Stress–strain relationship*

Based on Hooke's law, the stress–strain relations of the functionally graded circular microplate under uniformly distributed external pressure and thermal loading are given by [48]:

$$\left\{ \begin{matrix} \sigma_r \\ \sigma_\theta \end{matrix} \right\} = \left[\begin{matrix} Q_{11} & Q_{12} \\ Q_{21} & Q_{22} \end{matrix} \right] \left\{ \left\{ \begin{matrix} \varepsilon_r \\ \varepsilon_\theta \end{matrix} \right\} - \left\{ \begin{matrix} \alpha(z)\Delta T \\ \alpha(z)\Delta T \end{matrix} \right\} \right\}, \tag{14}$$

where ΔT is the temperature rise above room temperature without thermal stress of the structure and Q_{ij} is the reduced stiffness of the structure determined as follows:

$$Q_{11} = Q_{22} = \frac{E(z)}{1-\nu^2}, \quad Q_{12} = Q_{21} = \frac{E(z)\cdot\nu}{1-\nu^2}. \tag{15}$$

2.5. *Formulation of the energy equations*

The thermoelastic strain potential energy of the axially deformed FGM circular microplate is computed as follows [49]:

$$\begin{aligned} U_{\text{int}} &= \frac{1}{2}\int_V \left[\sigma_r\left(\varepsilon_r-\alpha\Delta T\right)+\sigma_\theta\left(\varepsilon_\theta-\alpha\Delta T\right)+2m_{r\theta}\chi_{r\theta}\right]\mathrm{d}V \\ &= \frac{1}{2}\int_V \left(\sigma_r\varepsilon_r+\sigma_\theta\varepsilon_\theta\right)\mathrm{d}V+\frac{1}{2}\int_V 2m_{r\theta}\chi_{r\theta}\mathrm{d}V-\frac{1}{2}\int_V\left(\sigma_r\alpha\Delta T+\sigma_\theta\alpha\Delta T\right)\mathrm{d}V \\ &= \pi\int_{-h/2}^{h/2}\int_0^a\left(\sigma_r\varepsilon_r+\sigma_\theta\varepsilon_\theta\right)r\mathrm{d}r\mathrm{d}z+2\pi\int_{-h/2}^{h/2}\int_0^a m_{r\theta}\chi_{r\theta}r\mathrm{d}r\mathrm{d}z \\ &\quad -\pi\Delta T\int_{-h/2}^{h/2}\int_0^a\alpha\left(\sigma_r+\sigma_\theta\right)r\mathrm{d}r\mathrm{d}z. \end{aligned} \tag{16}$$

Substituting Equations (12) and (14) into Equation (16), we obtain:

$$\begin{aligned} U_{\text{int}} &= \pi\int_{-h/2}^{h/2}\int_0^a\left(Q_{11}u_{,r}+\frac{1}{2}Q_{11}{w_{,r}}^2-Q_{11}zw_{,rr}+Q_{12}\frac{u}{r}-Q_{12}z\frac{w_{,r}}{r}\right)\left(u_{,r}+\frac{1}{2}{w_{,r}}^2-zw_{,rr}\right)r\mathrm{d}r\mathrm{d}z \\ &\quad +\pi\int_{-h/2}^{h/2}\int_0^a\left(Q_{21}u_{,r}+\frac{1}{2}Q_{21}{w_{,r}}^2-Q_{21}zw_{,rr}+Q_{22}\frac{u}{r}-Q_{22}z\frac{w_{,r}}{r}\right)\left(\frac{u}{r}-\frac{z}{r}w_{,r}\right)r\mathrm{d}r\mathrm{d}z \\ &\quad +2\pi\int_{-h/2}^{h/2}\int_0^a\frac{1}{2}Gl^2\left(\frac{1}{r}w_{,r}-w_{,rr}\right)^2r\mathrm{d}r\mathrm{d}z \\ &\quad -\pi\Delta T\int_{-h/2}^{h/2}\int_0^a\left[\alpha\left(Q_{11}+Q_{12}\right)\left(u_{,r}+\frac{1}{2}{w_{,r}}^2+\frac{u}{r}\right)-\alpha\left(Q_{11}+Q_{12}\right)z\left(w_{,rr}+\frac{w_{,r}}{r}\right)\right]r\mathrm{d}r\mathrm{d}z. \end{aligned} \tag{17}$$

The work performed by the external forces is given by [50]:

$$U_{\text{ext}} = 2\pi\int_0^a qwr\mathrm{d}r. \tag{18}$$

The total energy is obtained by combining Equations (17) and (18) as follows:

$$U_{\text{total}} = U_{\text{int}} - U_{\text{ext}}. \tag{19}$$

2.6. *Boundary conditions, solution form, and the Ritz energy method*

The axisymmetric FGM circular microplate with clamped boundary conditions along its perimeter is expressed as follows:

$$\begin{aligned} &\text{At } r=0: u=0, \quad w=\text{finite}, \quad w_{,r}=0. \\ &\text{At } r=a: u=0, \quad w=0, \quad w_{,r}=0. \end{aligned} \tag{20}$$

To enforce the boundary conditions given in Equation (20), the displacement and rotation fields are approximated by the following expressions:

$$u = U\frac{r(a-r)}{a^2}, \quad w = W\frac{\left(a^2-r^2\right)^2}{a^4} \tag{21}$$

where the amplitudes of the in-plane displacement u and the transverse deflection w are denoted by U and W, respectively.

The application of the Ritz energy approach to the total energy expression in Equation (19), after inserting the displacement fields given in Equation (21), leads to:

$$\frac{\partial U_{\text{total}}}{\partial U} = \frac{\partial U_{\text{total}}}{\partial W} = 0. \tag{22}$$

The relations in Equation (22), when treated using the Ritz energy approach, lead to a coupled system of two algebraic equations for the unknown coefficients U and W:

$$2a_{11}U + a_{13}W + a_{15}W^2 = 0, \tag{23}$$

$$2\left(a_{12} + a_{21} + a_{31}\Delta T\right)W + a_{13}U + 3a_{14}W^2 + 2a_{15}UW + 4a_{16}W^3 - Aq = 0 \tag{24}$$

where the coefficients are determined as follows:

$$a_{11} = \frac{\pi}{4}\int_{-h/2}^{h/2} Q_{11}\mathrm{d}z, \qquad a_{12} = \frac{32\pi}{3a^2}\int_{-h/2}^{h/2} Q_{11}z^2\mathrm{d}z,$$

$$a_{13} = \frac{16\pi}{5a}\int_{-h/2}^{h/2} Q_{11}z\mathrm{d}z, \qquad a_{14} = \frac{8\pi}{5a^2}\int_{-h/2}^{h/2} Q_{12}z\mathrm{d}z,$$

$$a_{15} = \left(\frac{82\pi}{315a}\int_{-h/2}^{h/2} Q_{12}\mathrm{d}z - \frac{46\pi}{315a}\int_{-h/2}^{h/2} Q_{11}\mathrm{d}z\right), \quad a_{16} = \frac{32\pi}{105a^2}\int_{-h/2}^{h/2} Q_{11}\mathrm{d}z,$$

$$a_{21} = \frac{32\pi}{3a^2}\int_{-h/2}^{h/2} Gl^2\mathrm{d}z, \qquad a_{31} = \frac{-\pi}{3}\int_{-h/2}^{h/2} \alpha\left(Q_{11} + Q_{12}\right)\mathrm{d}z, \qquad A = \frac{\pi a^2}{3}.$$

Solving Equation (23), the expression for the amplitude U is obtained as follows:

$$U = -\frac{a_{13}W + a_{15}W^2}{2a_{11}}. \tag{25}$$

Substituting the expression of U from Equation (25) into Equation (24), the resulting equation is:

$$\left(4a_{16} - \frac{{a_{15}}^2}{a_{11}}\right)W^3 + \left(3a_{14} - \frac{3a_{13}a_{15}}{2a_{11}}\right)W^2 + 2\left(a_{12} + a_{21} - \frac{{a_{13}}^2}{2a_{11}}\right)W + 2a_{31}\Delta TW - Aq = 0. \tag{26}$$

Equation (26) represents the relationship between the external pressure load q, the thermal load ΔT, and the deflection amplitude W. From this equation, the expressions for the external pressure q and the uniformly increased temperature ΔT are obtained as follows:

$$q = \frac{1}{A}\left(4a_{16} - \frac{{a_{15}}^2}{a_{11}}\right)W^3 + \frac{1}{A}\left(3a_{14} - \frac{3a_{13}a_{15}}{2a_{11}}\right)W^2 + \frac{2}{A}\left(a_{12} + a_{21} - \frac{{a_{13}}^2}{2a_{11}}\right)W + \frac{2a_{31}}{A}\Delta TW, \tag{27}$$

$$\Delta T = -\frac{1}{2a_{31}}\left(4a_{16} - \frac{{a_{15}}^2}{a_{11}}\right)W^2 - \frac{1}{2a_{31}}\left(3a_{14} - \frac{3a_{13}a_{15}}{2a_{11}}\right)W - \frac{1}{a_{31}}\left(a_{12} + a_{21} - \frac{{a_{13}}^2}{2a_{11}}\right) + \frac{Aq}{2a_{31}W}. \tag{28}$$

Equations (27) and (28) serve as the basis for analyzing the nonlinear thermo-mechanical post-buckling response of the FGM circular microplate.

The critical thermal buckling load according to the bifurcation criterion is derived by letting $W \to 0$ in Equation (28), yielding:

$$\Delta T_{\mathrm{cr}} = -\frac{1}{a_{31}}\left(a_{12} + a_{21} - \frac{{a_{13}}^2}{2a_{11}}\right). \tag{29}$$

For computational convenience, the following nondimensional transformations are introduced [51]:

$$q = \frac{QEh^4}{a^4}, \quad w_0 = \frac{w}{h}, \quad W_0 = \frac{W}{h}. \tag{30}$$

3. Comparative study

To verify the reliability of the methodology used in this study, a comparison between the nondimensional deflection amplitude of the FGM circular microplate and the results reported by Wang et al. [51] is presented in Table 1. Wang's findings were achieved by using the principle of minimum total energy to formulate nonlinear differential equations, converting these equations into nonlinear algebraic equations by the orthogonal collocation method, and resolving them using the Newton-Raphson iterative technique. A nondimensional transformation was implemented

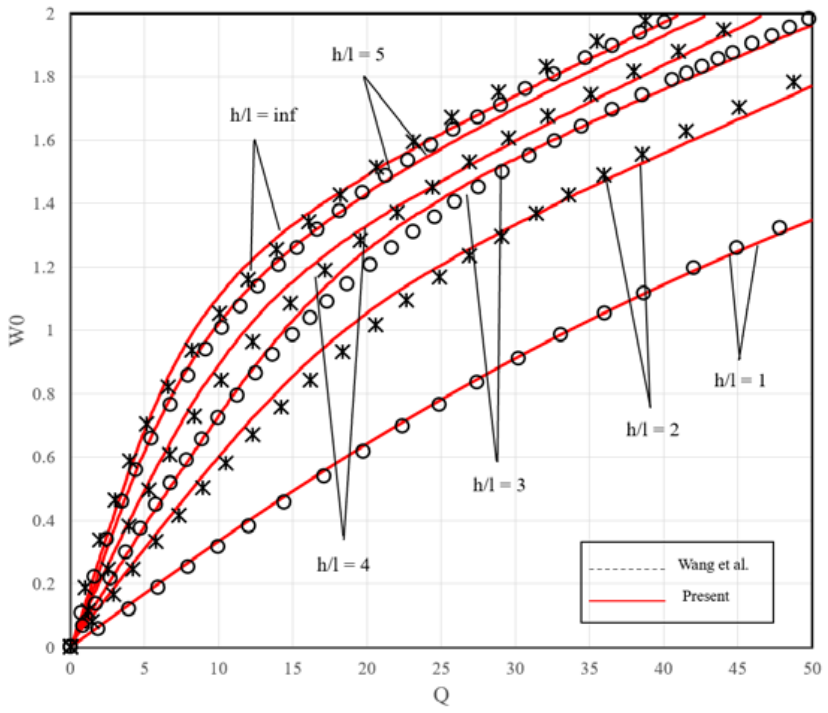

Figure 4. Comparison of the load-nondimensional deflection amplitude curves.

Table 1. Comparison of the nondimensional deflection amplitude $W_0 = w/h$ of an isotropic circular microplate subjected to a uniformly distributed external pressure ($\nu = 0.3$, $Q = 25$)

h/l	15	10	5	4	3	2	1
Wang et al. [51]	1.64643	1.64033	1.60713	1.58201	1.52748	1.37355	0.77189
This paper	1.57875	1.57269	1.54007	1.51578	1.46389	1.32114	0.76269
Difference (%)	4.11	4.12	4.17	4.19	4.16	3.82	1.19

for the evenly distributed load $q = QEh^4/a^4$. The comparison demonstrates a near alignment, with a maximum divergence of 4.19%. Consequently, this comparison substantiates the validity of the methodology used in the current study.

Next, we compare the load–deflection curves from Wang's study [51] with those from this study in Figure 4. The results are very similar, which shows that the two methods agree very well and confirms that the method used in this study is accurate and reliable.

4. Results and discussion

The numerical values presented in the Tables are obtained by directly substituting the specified material properties, geometric parameters, and intrinsic length-scale values into the derived closed-form analytical expressions. After performing the nondimensional transformations, the resulting algebraic equations are evaluated numerically using standard computational procedures. No additional numerical approximation schemes are employed beyond the direct evaluation of the analytical formulas.

Table 2. Influence of the ratios l/h, a/h, and the volume fraction index k on the critical thermal buckling load of the FGM circular microplate (E_c = 200 GPa; E_m = 70 GPa; $\alpha_c = 10 \times 10^{-6}$ 1/K; $\alpha_m = 23 \times 10^{-6}$ 1/K; $\nu = 0.3$; $a = 10^{-6}$ m)

l/h	a/h	k					
		0.1	1	3	5	7	10
0	20	480.1651	326.6435	282.7099	281.9525	280.5594	276.2116
	30	213.4067	145.1749	125.6488	125.3122	124.6930	122.7607
	40	120.0412	81.6608	70.6774	70.4881	70.1398	69.0529
0.2	20	562.6910	391.0799	334.4274	329.1014	325.3568	319.0505
	30	250.0848	173.8133	148.6344	146.2673	144.6030	141.8002
	40	140.6727	97.7699	83.6068	82.2753	81.3392	81.3392
0.5	20	995.9519	729.3710	605.9445	576.6330	560.5432	543.9549
	30	442.6453	324.1649	269.3086	256.2813	249.1303	241.7577
	40	248.9879	182.3427	151.4861	144.1582	140.1358	135.9887
1	20	2543.3125	1937.5534	1575.6483	1460.6743	1400.4945	1347.1848
	30	1130.3611	861.1348	700.2881	649.1886	622.4420	598.7488
	40	635.8281	484.3883	393.9120	365.1685	350.1236	336.7962

Table 2 shows that the critical thermal buckling load increases markedly with increasing l/h and decreasing a/h. Moreover, increasing the volume fraction index k reduces the critical buckling load due to reduced stiffness and a higher thermal expansion coefficient.

It should be noted that the present formulation is based on the classical Kirchhoff plate theory, which neglects transverse shear deformation. This assumption is appropriate for thin microplates with sufficiently large slenderness ratios. In the present study, the investigated range of thickness ratios is $a/h = 20 \div 40$, corresponding to thin and very thin plates, for which shear effects are generally negligible. However, for moderately thick microplates with $a/h < 20$, transverse shear deformation may become significant, and higher-order shear deformation theories (e.g., Mindlin or HSDT models) would be more appropriate. Such extensions may be considered in future work.

The graphical results presented in this study are generated directly from the closed-form analytical expressions derived in the previous sections. For each case, the specified material properties, geometric parameters, and intrinsic length-scale values are substituted into the nondimensional governing equations to compute the corresponding numerical values. The resulting data are then processed and plotted using MATLAB. No experimental data or independent numerical simulations are employed in constructing the figures.

Figures 5a and 5b illustrate the inverse relationship between the critical thermal buckling temperature ΔT_{cr} and the volume fraction index k. It is evident that for any values of the ratios l/h and a/h, ΔT_{cr} decreases rapidly as k increases from 0 to approximately 2–4, after which the rate of decrease gradually slows and approaches an asymptotic trend for larger values of k. This indicates that increasing the metallic volume fraction (i.e., increasing k) significantly reduces the thermal stability of the structure.

Figures 5c and 5d confirm the trends identified in Table 2. Figure 5c shows that the critical thermal buckling temperature increases strongly and nonlinearly with increasing l/h, with the size effect becoming particularly pronounced for $l/h > 0.2$. Figure 5d illustrates the inverse relationship between ΔT_{cr} and a/h, indicating that plates with larger surface areas (i.e., increasing a) or thinner thicknesses (i.e., decreasing h) exhibit lower thermal stability.

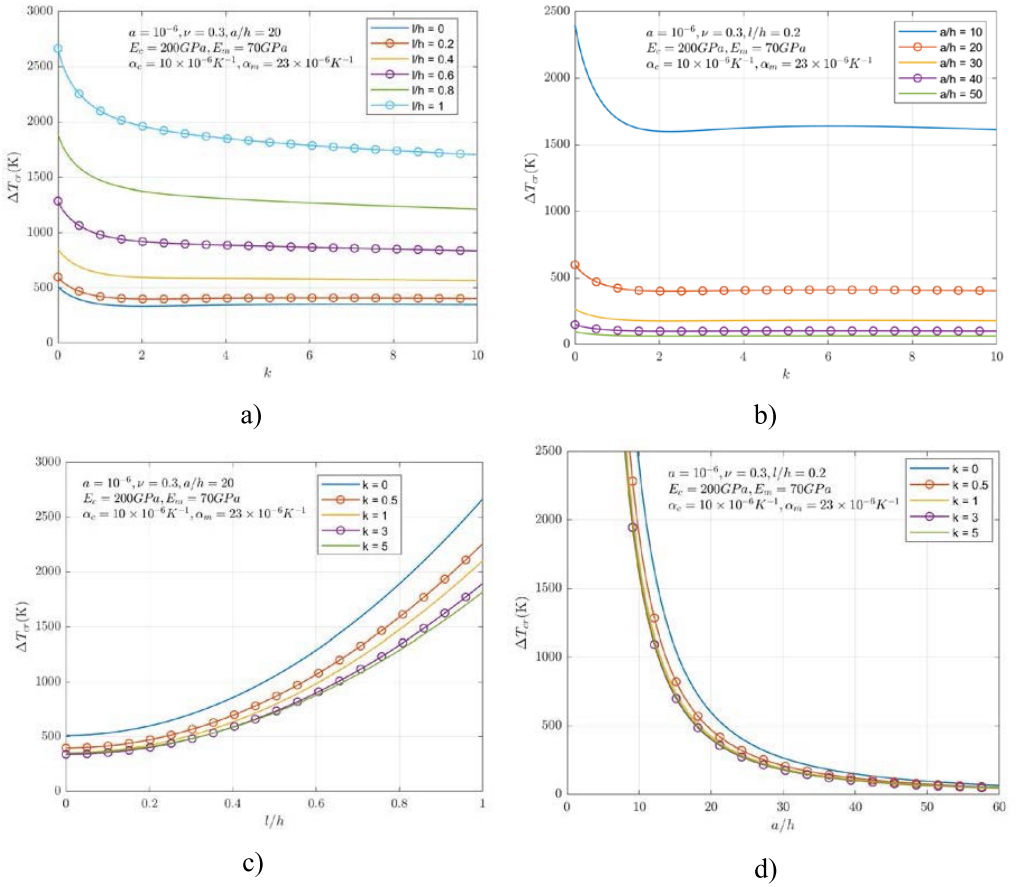

Figure 5. Relationship of the ratios l/h, a/h, and the volume fraction index k to the critical thermal buckling load of the FGM circular microplate.

From the results in Table 2 and the plots in Figure 5, it is observed that the critical thermal buckling temperature ΔT_{cr} of the FGM circular microplate is generally lower than that of a homogeneous circular microplate. That is, the thermal stability of the FGM circular microplate is inferior to that of a fully ceramic microplate (i.e., when $k = 0$).

The influence of the FGM volume fraction index k on the post-buckling thermo-mechanical behavior is presented in Figures 6a and 6b. The post-buckling mechanical and thermal load-carrying capacities of the FGM circular microplate increase as the volume fraction index k decreases. Figure 6a illustrates the thermal response; the temperature–deflection curves indicate that the post-buckling thermal resistance decreases sharply as k increases. Plates with smaller k values (i.e., ceramic-rich compositions) retain stiffness and stability much better under thermal loading compared to plates with larger k values (i.e., metal-rich compositions). Figure 6b shows the mechanical response; the load–deflection curves reveal a reduction in post-buckling mechanical resistance as k increases. At an ambient temperature increase of $\Delta T = 400$ K, an initial deflection occurs prior to the application of external pressure for $k = 1, 3, 5$.

In both cases examined in Figure 7, it is evident that as the ratio a/h increases (i.e., the plate becomes wider and thinner), the post-buckling mechanical and thermal load-carrying capacities decrease. The curves corresponding to $a/h = 40$ lie significantly lower than those for $a/h = 20$ and $a/h = 30$, indicating that the slenderness of the plate has a strong influence on its post-buckling resistance.

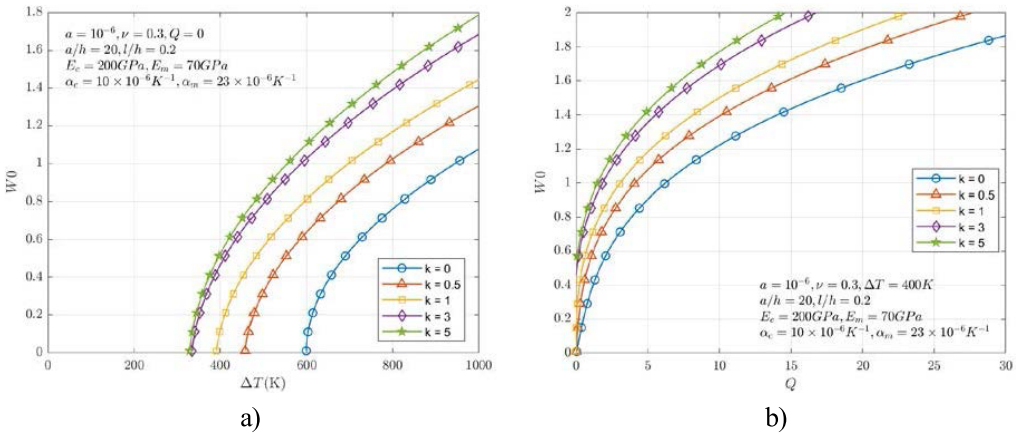

Figure 6. Influence of the volume fraction index k on the post-buckling mechanical and thermal behavior of the FGM circular microplate.

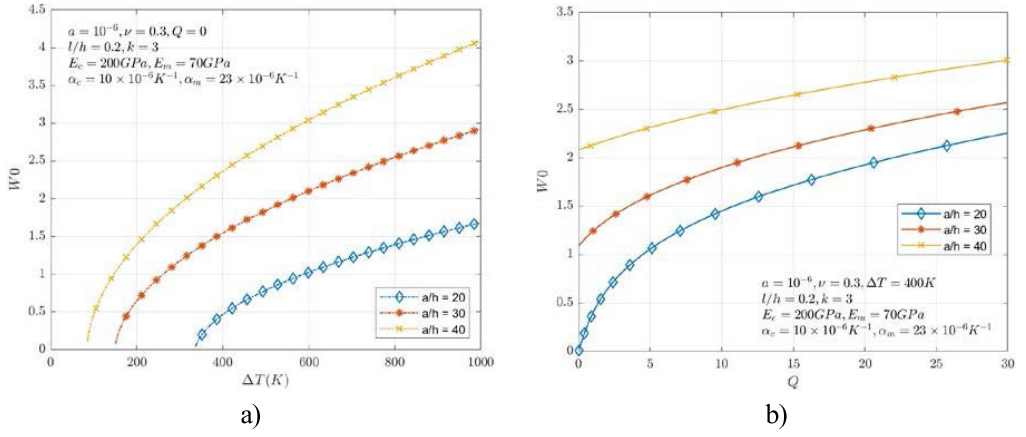

Figure 7. Influence of the ratio a/h on the post-buckling mechanical and thermal behavior of the FGM circular microplate.

Figure 8 illustrates the influence of the ratio l/h on the post-buckling thermo-mechanical behavior. The post-buckling mechanical and thermal load-carrying capacities of the FGM circular microplate decrease as the ratio l/h decreases. The findings indicate that the material characteristic length parameter enhances the stiffness, thereby reducing the deflection of the FGM circular microplate. However, the size effect becomes significant only when l/h is large and gradually diminishes as this ratio approaches zero (i.e., the classical model). Moreover, at an ambient temperature increase of $\Delta T = 400$ K, an initial deflection appears before the application of external pressure for the cases $l/h = 0$ and $l/h = 0.2$.

In both cases examined in Figure 9, it is observed that the deflection increases nonlinearly with the radial coordinate r/a, and the load-carrying capacity of the structure increases as the ratio l/h increases or a/h decreases. Figure 9a shows that the influence of l/h on the deflection is significant when l/h is large, but it decreases markedly and may be neglected when l/h is small. Therefore, plates modeled using the modified couple stress theory exhibit greater stiffness compared to those modeled using the classical plate theory (i.e., $l = 0$). Figure 9b presents the influence of a/h; for the same load level, plates with larger a/h values exhibit higher deflections, which is consistent with the observation that more slender structures deform more easily.

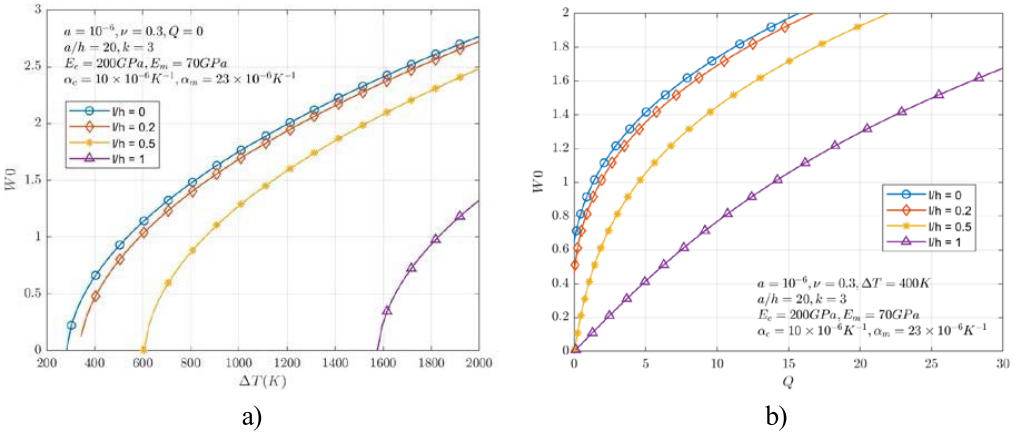

Figure 8. Influence of the ratio l/h on the post-buckling mechanical and thermal behavior of the FGM circular microplate.

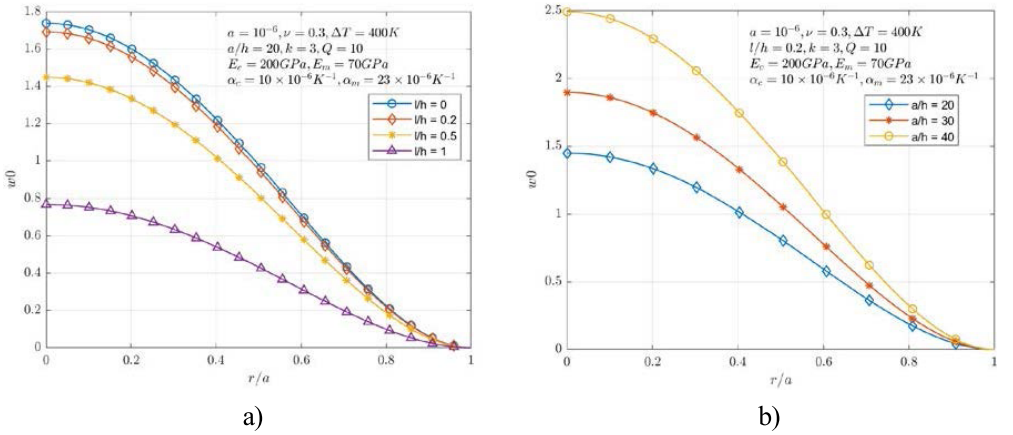

Figure 9. Nondimensional deflection curves w_0 along the radial coordinate r/a.

Analysis reveals that the material length-scale parameter l in the modified couple stress theory plays a crucial role in enhancing stiffness and buckling stability. Additionally, it should be acknowledged that at the micro-scale, the intrinsic length scale may interact with thermal processes, thereby influencing heat conduction paths and the distribution of localized thermal deformation [15,26]. This work is limited to the aspects of nonlinear mechanics and pure size effects. For further expansion, future studies could incorporate the temperature dependence of parameter l or apply advanced heat conduction models to more fully elucidate this complex multiphysical relationship.

Figure 10a illustrates the effect of mechanical loading on the temperature–deflection curve. As the applied mechanical load increases, the temperature–deflection curve shifts upward, indicating that under combined mechanical and thermal loading, the structure becomes unstable at a lower temperature compared to the case of pure thermal loading. Figure 10b depicts the influence of thermal loading on the load–deflection curve. The load–deflection curves shift downward as ΔT decreases, demonstrating that the mechanical response of the structure is significantly reduced under the influence of temperature.

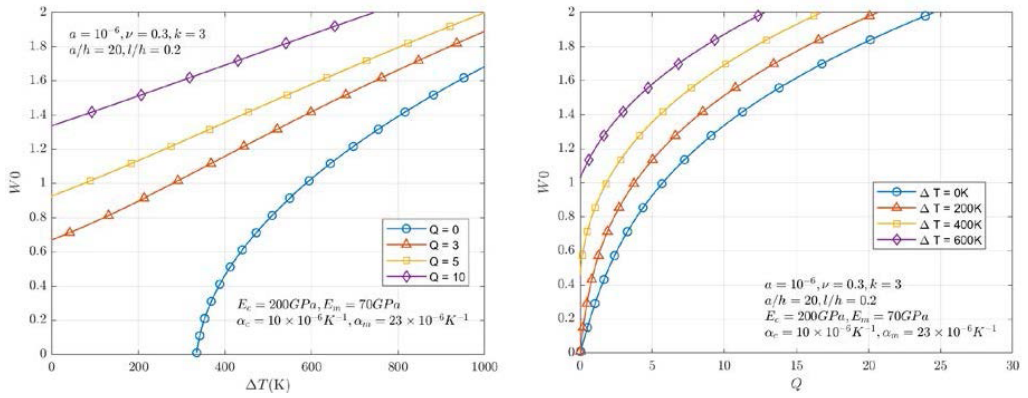

Figure 10. Influence of mechanical loading on the thermal response and influence of thermal loading on the mechanical post-buckling response. (a) Influence of mechanical loading on the post-buckling thermal response. (b) Influence of thermal loading on the post-buckling mechanical response.

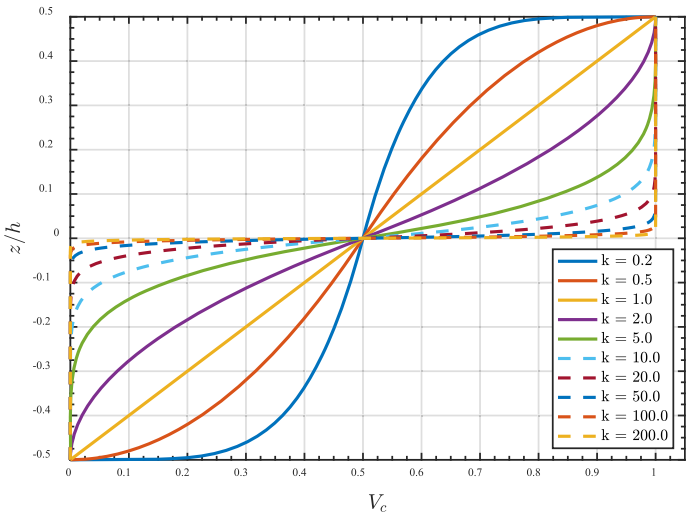

Figure 11. Variation of V_c through the thickness based on the Sigmoid distribution.

Figure 12 presents a comparative analysis of the influence of different FGM volume fraction distribution laws on the post-buckling thermo-mechanical behavior. We further consider the Sigmoid distribution pattern as expressed in Equations (31) and (32).

$$V_c = 1 - \frac{1}{2}\left(\frac{h/2 - z}{h/2}\right)^k \quad \text{where } 0 \le z \le h/2 \tag{31}$$

$$V_c = \frac{1}{2}\left(\frac{h/2 + z}{h/2}\right)^k \quad \text{where } -h/2 \le z \le 0. \tag{32}$$

Variation of V_c through the thickness based on the Sigmoid distribution is presented in Figure 11.

Figure 12a illustrates the effect of mechanical loading on the post-buckling thermal response under two different distribution laws. The temperature–deflection curves for the two distribution

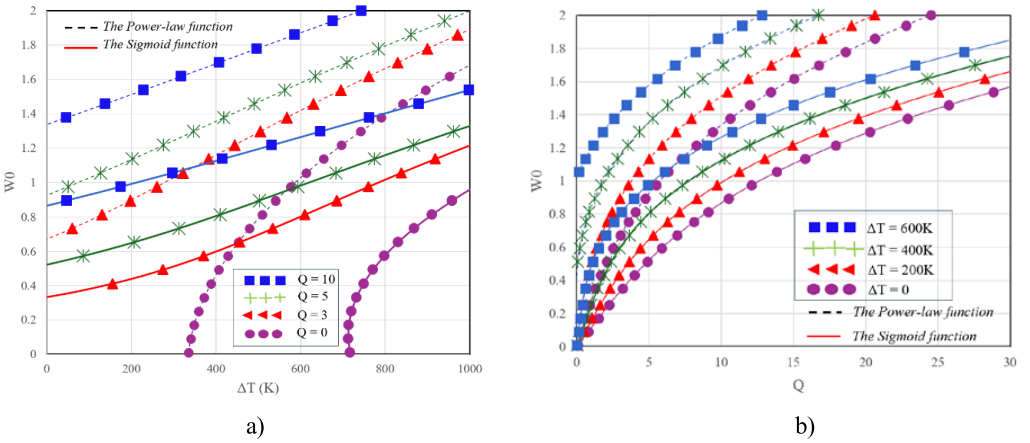

Figure 12. Combined influence of mechanical and thermal loading on the post-buckling behavior for two different volume fraction distribution laws. (a) Influence of mechanical loading on the post-buckling thermal response for two different volume fraction distribution laws. (b) Influence of thermal loading on the post-buckling mechanical response for two different volume fraction distribution laws.

laws differ significantly. This indicates that the thermal resistance of the structure depends not only on the volume fraction index k but also on the specific distribution pattern of the constituent materials along the thickness direction. Similarly, Figure 12b shows the influence of thermal loading on the post-buckling mechanical behavior. The differences between the load–deflection curves for the two distribution laws demonstrate that the distribution pattern significantly affects the structural stiffness and mechanical load-carrying capacity. Therefore, in addition to selecting the volume fraction index k, choosing an appropriate gradient distribution law for the FGM is an important factor in enhancing the load-bearing performance of FGM circular microplates under combined mechanical and thermal loading conditions.

The current model employs the Voigt rule of mixtures for the sake of simplicity. Future research could incorporate more advanced micromechanical homogenization methods, such as the Mori–Tanaka scheme, to obtain more accurate effective material properties for FGMs, particularly when the constituent phases possess significantly different elastic moduli.

5. Conclusion

In this study, the nonlinear static buckling behavior of functionally graded circular microplates is analyzed by combining Kirchhoff plate theory, von Kármán geometric nonlinearity, and the modified couple stress theory. The structure is concurrently subjected to a uniformly distributed external pressure and a uniformly rising through-thickness thermal load. Using a displacement-based approach, the assumed forms of the displacement and deflection components were expressed as polynomial functions that satisfy the clamped boundary conditions along the plate's perimeter. This choice of displacement fields reduces computational complexity while maintaining sufficient accuracy in evaluating the structural response under loading. By applying the Ritz energy method, explicit expressions for the critical thermal buckling load of the FGM circular microplate and the load–deflection relationships in the nonlinear post-buckling regime were derived. The results of the numerical analysis reveal that the FGM volume fraction index k, the material length scale parameter l, and geometric factors all play significant roles in determining the load-carrying capacity and post-buckling behavior of the structure. Adjusting these parameters

can optimize the structural design to enhance both mechanical and thermal post-buckling performance. These outcomes provide a scientific basis for the design and optimization of structures operating under real-world thermo-mechanical loading conditions.

Data availability

The data supporting the conclusions of this investigation are included in the text.

Acknowledgment

This paper is funded by the Le Quy Don Technical University Research Fund under code 25.01.14.

Declaration of interests

The authors do not work for, advise, own shares in, or receive funds from any organization that could benefit from this article, and have declared no affiliations other than their research organizations.

References

[1] D. Van Doan, P. Van Minh, T. Van Ke, N. T. C. Nhung and D. Van Thom, "An overview of functionally graded materials: from civil applications to defense and aerospace industries", *J. Vib. Eng. Technol.* **13** (2025), no. 1, article no. 68.

[2] J. Zhu et al., "Development trends and perspectives of future sensors and MEMS/NEMS", *Micromachines* **11** (2020), no. 1, article no. 7.

[3] R. Tiwari, S. Sachan, A. Abouelregal, R. Kumar and M. E. Elzayady, "Viscothermoelastic vibrations on circular microplate resonators using the MooreGibsonThompson thermal-conductivity model", *Mech. Time-Dependent Mater.* **28** (2024), no. 3, pp. 1291–1311.

[4] J. Lin, H. Liu, W. Shen and S. Gu, "Vibration energy harvesting in an FG-CNTRC circular microplate with a surface-bonded piezoelectric layer", *Eur. J. Mech. A Solids* **106** (2024), article no. 105325.

[5] A. E. Abouelregal, M. Marin, A. Foul and S. S. Askar, "Thermoviscoelastic responses in Kirchhoff circular microplate via mgt thermoelastic model and modified couple stress theory", *Mech. Solids* **59** (2024), no. 4, pp. 2269–2291.

[6] V. N. Van Do, T. H. Ong and C. H. Lee, "Nonlinear thermal buckling analysis of temperature-dependent porous annular and circular microplates reinforced by graphene platelets by using isogeometric analysis method", *Eng. Struct.* **305** (2024), article no. 117738.

[7] S. M. H. Hosseini, Y. Tadi Beni and Y. Kiani, "Vibration analysis of rotating annular flexoelectric microplate", *Int. J. Struct. Stab. Dyn.* **25** (2025), no. 12, article no. 2550126.

[8] C. Li and H. Aiqing, "Size-dependent axisymmetric buckling and free vibration of fgp-microplate using well-posed nonlocal integral polar models", *J. Mech. Mater. Struct.* **19** (2024), no. 3, pp. 323–341.

[9] N. Ahmadi, M. Fathalilou and G. Rezazadeh, "Neo-Hookean modeling of nonlinear coupled behavior in circular plates supported by micro-pillars", *Sci. Rep.* **14** (2024), no. 1, article no. 25428.

[10] Z. Yuan, X. F. Cheng, Z. Li, Y. Li and C. He, "Asymmetric optical waveguide in one-dimensional organic microplate", *Responsive Mater.* **3** (2025), no. 1, article no. e20240034.

[11] P. T. Hung, H. Nguyen-Xuan, P. Phung-Van and C. H. Thai, "Modified strain gradient analysis of the functionally graded triply periodic minimal surface microplate using isogeometric approach", *Eng. Comput.* **40** (2024), no. 5, pp. 2877–2904.

[12] Y. Harazono, H. Shimono, K. Hata, T. Mitsuyama and T. Horinouchi, "Evaluation of microplate handling accuracy for applying robotic arms in laboratory automation", *SLAS Technol.* **29** (2024), no. 6, article no. 100200.

[13] C. Xiao, G. Zhang, P. S. Hu, Y. Yu, Y. Y. Mo and V. Borjalilou, "Size-dependent generalized thermoelasticity model for thermoelastic damping in circular nanoplates", *Waves Random Complex Media* **34** (2024), no. 4, pp. 2795–2815.

[14] W. Peng, X. Zhang, Y. Gao, T. He and Y. Li, "Small-scale and memory-dependent effects on thermoelastic damping analysis of composite microplate resonators reinforced with graphene nanoplatelets", *Mech. Adv. Mater. Struct.* **31** (2024), no. 29, pp. 11436–11449.

[15] W. Peng, A. M. Zenkour, Y. Gao, X. Zhang, T. He and Y. Li, "Size-dependent thermoelastic damping analysis in functionally graded graphene nanoplatelets reinforced composite microplate resonators based on MooreGibson-Thompson thermoelasticity", *Z. Angew. Math. Mech.* **104** (2024), no. 8, article no. e202301091.

[16] L. Liu, F. Gao, B. Zhang, J. Liu, Y. Yang and H. Deng, "Symmetric/asymmetric vibrational characteristics of bi-directional functionally graded annular microplates", *Int. J. Struct. Stab. Dyn.* **25** (2025), no. 6, article no. 2550059.

[17] R. Ansari, T. Pourashraf, R. Gholami and H. Rouhi, "Analytical solution approach for nonlinear buckling and postbuckling analysis of cylindrical nanoshells based on surface elasticity theory", *Appl. Math. Mech.* **37** (2016), no. 7, pp. 903–918.

[18] R. Ansari, R. Gholami, M. Faghih Shojaei, V. Mohammadi and M. A. Darabi, "Thermal buckling analysis of a mindlin rectangular FGM microplate based on the strain gradient theory", *J. Therm. Stress.* **36** (2013), no. 5, pp. 446–465.

[19] Y. Gholami, R. Ansari, R. Gholami and F. Sadeghi, "Size-dependent free vibration and buckling analysis of magneto-electro-thermo-elastic nanoplates based on the third-order shear deformable nonlocal plate model", *Proc. Inst. Mech. Eng. C J. Mech. Eng. Sci.* **236** (2022), no. 14, pp. 8116–8133.

[20] V. Jain, R. Kumar, T. Dey, S. N. Patel and G. Watts, "A meshfree formulation for size-dependent thermal buckling and post-buckling behaviour of porous microplates on elastic foundation subjected to localized heating", *Thin-Walled Struct.* **205** (2024), article no. 112451.

[21] D. Chen, Q. Wang and Z. Zhang, "Buckling analysis of GPL RC micro smart plates resting on elastic foundation subjected to thermal loads", *Arch. Appl. Mech.* **95** (2025), no. 6, article no. 128.

[22] V. T. Tran, T. K. Nguyen and H. Nguyen-Xuan, "An intelligent computational iBCMO-DNN algorithm for stochastic thermal buckling analysis of functionally graded porous microplates using modified strain gradient theory", *J. Therm. Stress.* **47** (2024), no. 9, pp. 1188–1227.

[23] H. Liu, Q. Wang and Z. Zhang, "Thermal buckling of graphene platelets reinforced microplates with piezoelectric layers using artificial neural network", *Eng. Appl. Artif. Intell.* **150** (2025), article no. 110469.

[24] X. Zhang, C. Du, L. Li, J. Fang and D. Zhang, "Thermal buckling, vibration and transient response of rotating GNPs-reinforced porous microbeams in thermal environment", *Acta Mech. Sin.* **41** (2025), no. 10, article no. 524370.

[25] N. Joueid, S. Zghal, M. Chrigui and F. Dammak, "Thermoelastic buckling analysis of plates and shells of temperature and porosity dependent functionally graded materials", *Mech. Time-Depend. Mater.* **28** (2024), no. 3, pp. 817–859.

[26] X. Qin, N. Ben Kahla and N. Ghazouani, "Computer simulation for determination of critical buckling temperatures of sandwich microplates with cellular core and CNT-RC piezoelectric patches via MSGT", *Int. J. Struct. Stab. Dyn.* **25** (2025), no. 15, article no. 2550159.

[27] F. Tang, S. Shi, S. He, F. Dong and S. Liu, "Size-dependent vibration and buckling of porous functionally graded microplates based on modified couple stress theory in thermal environments by considering a dual power-law distribution of scale effects", *Appl. Math. Mech.* **45** (2024), no. 12, pp. 2075–2092.

[28] E. Salari and S. A. S. Vanini, "Nonlocal nonlinear static/dynamic snap-through buckling and vibration of thermally post-buckled imperfect functionally graded circular nanoplates", *Waves Random Complex Media* **35** (2025), no. 2, pp. 3805–3851.

[29] C. Liu, M. Chen, M. Habibi and X. Chen, "Effect of micro-scale parameter and thermal loads on the stress/strain/displacement distribution of micro-plate", *J. Vib. Eng. Technol.* **13** (2025), no. 1, article no. 130.

[30] P. Wen, B. Zhang, C. Li, Z. Peng, Y. Duan and X. Zhang, "Modeling and prediction of buckling mode transitions in double-layered microplate systems with couple stress effects and interlayer interactions", *Mech. Adv. Mater. Struct.* (2025), pp. 1–23.

[31] V. T. Tran, T. K. Nguyen, V. H. Nguyen and T. P. Vo, "Novel computational algorithms for vibration, buckling, and transient analysis of porous metal foam microplates", *J. Vib. Eng. Technol.* **13** (2025), no. 3, article no. 203.

[32] A. A. Daikh, M. S. A. Houari and A. Tounsi, "Buckling analysis of porous FGM sandwich nanoplates due to heat conduction via nonlocal strain gradient theory", *Eng. Res. Express* **1** (2019), no. 1, article no. 015022.

[33] A. Farajpour, M. R. H. Yazdi, A. Rastgoo and M. Mohammadi, "A higher-order nonlocal strain gradient plate model for buckling of orthotropic nanoplates in thermal environment", *Acta Mech.* **227** (2016), no. 7, pp. 1849–1867.

[34] M. Bouazza, "Analytical modeling for the thermoelastic buckling behavior of functionally graded rectangular plates using hyperbolic shear deformation theory under thermal loadings", *Multidiscip. Model. Mater. Struct.* **5** (2009), no. 1, pp. 59–76.

[35] D. Khuat Duc, L. Nguyen Tuan, M. Dao Nhu, N. T. Hong, T. Van Ke and P. Van Minh, "A novel isogeometric model for dynamic buckling analysis of doubly curved two-directional functionally graded porous shallow microshells in thermal environments via variable length-scale parameters", *Mech. Based Des. Struct. Mach.* **52** (2024), no. 11, pp. 8610–8638.

[36] F. L. Li, S. J. Fan, Y. Q. Hao and M. Lv, "Analysis of vibro-acoustic characteristics of functionally graded sandwich microplates under thermal-electric effects", *J. Intell. Mater. Syst. Struct.* **35** (2024), no. 8, pp. 760–774.

[37] M. I. Marin, R. P. Agarwal and I. A. Abbas, "Effect of intrinsic rotations, microstructural expansion and contractions in initial boundary value problem of thermoelastic bodies", *Bound. Value Probl.* **2014** (2014), article no. 129.

[38] S. Vlase, I. Negrean, M. Marin and M. L. Scutaru, "Energy of accelerations used to obtain the motion equations of a three-dimensional finite element", *Symmetry* **12** (2020), no. 2, article no. 321.

[39] A. E. Abouelregal, M. Marin and A. Öchsner, "The influence of a non-local Moore-Gibson-Thompson heat transfer model on an underlying thermoelastic material under the model of memory-dependent derivatives", *Contin. Mech. Thermodyn.* **35** (2023), no. 2, pp. 545–562.

[40] F. Yang, A. C. M. Chong, D. C. C. Lam and P. Tong, "Couple stress based strain gradient theory for elasticity", *Int. J. Solids Struct.* **39** (2002), no. 10, pp. 2731–2743.

[41] H. M. Ma, X. L. Gao and J. N. Reddy, "A microstructure-dependent Timoshenko beam model based on a modified couple stress theory", *J. Mech. Phys. Solids* **56** (2008), no. 12, pp. 3379–3391.

[42] G. C. Tsiatas, "A new Kirchhoff plate model based on a modified couple stress theory", *Int. J. Solids Struct.* **46** (2009), no. 13, pp. 2757–2764.

[43] G. N. Praveen and J. N. Reddy, "Nonlinear transient thermoelastic analysis of functionally graded ceramic-metal plates", *Int. J. Solids Struct.* **35** (1998), no. 33, pp. 4457–4476.

[44] R. C. Wetherhold, S. Seelman and J. Wang, "The use of functionally graded materials to eliminate or control thermal deformation", *Compos. Sci. Technol.* **56** (1996), no. 9, pp. 1099–1104.

[45] Y. Tanigawa, H. Morishita and S. Ogaki, "Derivation of systems of fundamental equations for a three-dimensional thermoelastic field with nonhomogeneous material properties and its application to a semi-infinite body", *J. Therm. Stress.* **22** (1999), no. 7, pp. 689–711.

[46] S. Kapuria and P. C. Dumir, "Geometrically nonlinear axisymmetric response of thin circular plate under piezoelectric actuation", *Commun. Nonlinear Sci. Numer. Simul.* **10** (2005), no. 4, pp. 411–423.

[47] M. Haterbouch and R. Benamar, "Geometrically nonlinear free vibrations of simply supported isotropic thin circular plates", *J. Sound Vib.* **280** (2005), no. 3-5, pp. 903–924.

[48] M. Ghadiri, M. Mahinzare, N. Shafiei and K. Ghorbani, "On size-dependent thermal buckling and free vibration of circular FG Microplates in thermal environments", *Microsyst. Technol.* **23** (2017), no. 10, pp. 4989–5001.

[49] L. L. Ke, J. Yang, S. Kitipornchai, M. A. Bradford and Y. S. Wang, "Axisymmetric nonlinear free vibration of size-dependent functionally graded annular microplates", *Compos. Part B Eng.* **53** (2013), pp. 207–217.

[50] I. Eshraghi, S. Dag and N. Soltani, "Consideration of spatial variation of the length scale parameter in static and dynamic analyses of functionally graded annular and circular micro-plates", *Compos. Part B Eng.* **78** (2015), pp. 338–348.

[51] Y. G. Wang, W. H. Lin and C. L. Zhou, "Nonlinear bending of size-dependent circular microplates based on the modified couple stress theory", *Arch. Appl. Mech.* **84** (2014), no. 3, pp. 391–400.